energies

MDPI

Article

A Real-Time Bi-Adaptive Controller-Based Energy Management System for Battery–Supercapacitor Hybrid Electric Vehicles

Sadam Hussain [1], Muhammad Umair Ali [1], Gwan-Soo Park [1], Sarvar Hussain Nengroo [1], Muhammad Adil Khan [2] and Hee-Je Kim [1,*]

[1] School of Electrical Engineering, Pusan National University, Busandaehak-ro 63beon-gil, Geumjeong-gu, Busan 46241, Korea; sadamengr15@gmail.com (S.H.); umairali.m99@gmail.com (M.U.A.); gspark@pusan.ac.kr (G.-S.P.); ssarvarhussain@gmail.com (S.H.N.)

[2] Department of Electrical and Computer Engineering, Air University, Islamabad 44000, Pakistan; adil.khan@mail.au.edu.pk

* Correspondence: heeje@pusan.ac.kr; Tel.: +82-10-2754-4587 or +82-51-510-2364

Received: 22 October 2019; Accepted: 5 December 2019; Published: 8 December 2019

check for updates

Abstract: The energy storage system (ESS) is the main issue in traction applications, such as battery electric vehicles (BEVs). To alleviate the shortage of power density in BEVs, a hybrid energy storage system (HESS) can be used as an alternative ESS. HESS has the dynamic features of the battery and a supercapacitor (SC), and it requires an intelligent energy management system (EMS) to operate it effectively. In this study, a real-time EMS is proposed, which is comprised of a fuzzy logic controller-based low-pass filter and an adaptive proportional integrator-based charge controller. The proposed EMS intelligently distributes the required power from the battery and SC during acceleration. It allocates the braking energy to the SC on the basis of the state of charge. A simulation study was conducted for three standard drive cycles (New York City cycle, Artemis urban cycle, and New York composite cycle) using MATLAB Simulink. Comparative analysis of conventional and proposed EMSs was carried out. The results reveal that the proposed EMS reduced the stress, temperature, and power losses of the battery. The steady-state charging performance of the SC was 98%, 95%, and 96% for the mentioned drive cycles.

Keywords: energy management system; adaptive controller; semi-active hybrid energy storage system; electric vehicle; battery; supercapacitor

1. Introduction

The transportation sector plays a key role in energy consumption and greenhouse gas emissions, triggering global warming with limited fossil fuel resources and price fluctuations, which leads to the need for investigating an alternate energy source [1,2]. Therefore, attention has shifted to battery electric vehicles (BEVs) [3]. A BEV provides a high energy density, which looks like an ideal solution for reducing the energy of the transport sector and gas emissions [4]. However, it brings some challenges; for instance, the requirement of a high-power energy storage system (ESS) that can satisfy the power requirements during acceleration and efficiently recover energy during deceleration without the deterioration in the life cycle and efficiency of the ESS [5,6]. Thus, the practice of using a battery alone as an ESS is highly vulnerable to the high power demand of the electric vehicle caused by variable driving road and traffic conditions, which compromises the battery life and performance, and induces battery aging [7–9].

To address this problem, an alternate ESS is required for BEVs to overcome the challenges of the battery. Supercapacitors (SCs) can be used as a secondary source, which has a higher charging/discharging efficiency, high power density, and a longer lifespan compared to batteries [10,11]. Figure 1 presents the comparison between the power and energy density of different ESSs in a Ragone plot [12]. A hybrid ESS (HESS) has a combination of two storage elements having high-energy and high-power to increase the overall specific energy and specific power [13].

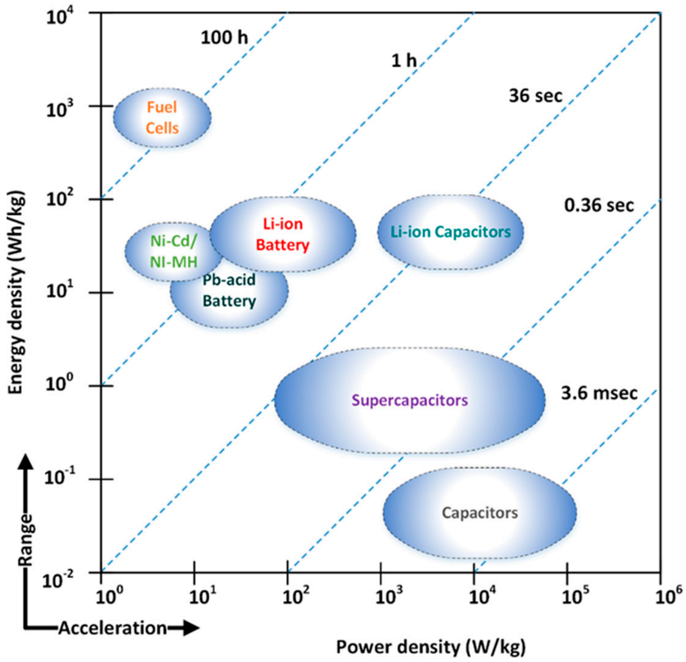

Figure 1. Ragone plot of the few energy storage devices used in electric vehicle applications.

In general, there are three main categories of HESSs, i.e., passive HESS, semi-active HESS, and fully active HESS [14]. In a passive HESS, different ESSs are connected in parallel to each other without any converter directly coupled to the DC bus [15]. A passive HESS is very simple and cost-effective, but there is no control algorithm involved in this system [11]. In contrast, a fully active HESS has the best control topology because each ESS has its own converter [16,17]. However, this topology demands a high cost, is heavyweight, has a large size, is less efficient, and has complicated control circuitry [18]. Compared with the above two topologies, a semi-active HESS is a good tradeoff between performance and system cost because it involves only one bi-directional DC–DC converter. Because of these advantages, a semi-active HESS is the preferred topology to use [19,20].

By having two different ESSs, an intelligent and robust energy management system (EMS) is needed. In the literature, there are two main types of EMS for an HESS: An off-line strategy uses the advance optimization algorithms, for instance, particle swarm optimization, dynamic programming (DP), and genetic algorithm [21,22]. The other strategy is the real-time approach, such as rule-based methods, the model predictive control (MPC) method, and frequency-based methods. The off-line strategy is very complex, which requires complete load profile information in advance and the backward calculation process makes this strategy difficult to implement in practical applications [23]. The real-time strategy, on the other hand, is explicit and very easy to implement in onboard applications [24,25].

Previously, researchers have used different EMSs for hybrid electric vehicles (HEVs) [26–28]. In Santucci et al. [26], an HEV consisted of an HESS and an internal combustion engine that used the equivalent consumption minimization strategy with an MPC and DP algorithm. Masih et al. [27] used a similar HEV configuration as discussed in Santucci et al. [26], but the EMS used in their research was a fuzzy logic controller (FLC) and a DP algorithm was used to increase the battery life cycle. Similarly, Ansarery et al. [28] used an HEV composed of a fuel cell system and an HESS. A multi-dimensional DP algorithm was used as the EMS between the fuel cell and the HESS to decrease the hydrogen consumption. However, few studies aimed at the energy management of the HESS for a pure HEV. Kailong et al. [29] studied different techniques for a EMS with the discussion of the battery model in terms of the state of charge (SOC), the state of health, and the internal temperature of the battery. Song et al. [18] compared four EMSs, which are the filtrating-based controller, the rule-based controller, the MPC, and the FLC. The rule-based EMS implemented in References [16,30], which was based on expert experience, used a rule-based controller considered a load power and the SOC of an HESS to improve the range and the performance of the electric vehicle (EV). The rule-based method does not require any prior information about the drive cycle, but it does not consider the frequency components in load demand, which is very harmful to battery life. Also, these rules were analyzed based on the initial state of the HESS and cannot precisely reflect the conditions of the system components after a long period of operation. Therefore, the distribution of energy is an essential factor to ensure EVs over a long range and also to improve the battery life cycle [31]. Wang et al. [31] proposed an MPC for different energy sources to achieve the required energy distribution of an EV without prior knowledge of the drive cycles. Still, an MPC needs a highly accurate model. A nonlinear MPC was used as an EMS for an HESS in the real-time system and compared with linear MPC and a rule-based controller [32]. A frequency-based EMS considers the high- and low-frequency components in the load power demand, and two filters are used to achieve frequency separation [33]. Huang et al. [34] presented only two cut-off frequencies: the urban driving cycle mode and the highway driving cycle mode in a frequency-based EMS. Only two frequencies were proposed, i.e., a high frequency for the SC and a low frequency for the battery. However, the cut-off frequency in these cases is not adaptive and does not consider the specific changes in load power in different situations. The frequency distribution should be continuously updated to guarantee real driving conditions. Andersson et al. [35] implemented a fixed-frequency-based EMS with a proportional controller (FF-P) for the charging control of a SC, but the SOC of a SC is not strictly controlled and the power allocation does not update with variations in the drive cycle. Hamid et al. [36] studied an adaptive intelligent EMS for a HEV using FL, but required high memory for the optimization. Jamila et al. [37] used an adaptive FLC-based filtering strategy, but for controlling the SC, they used a sliding mode controller, which is a tedious and complicated task for the optimum sliding surface [38]. References [39,40] used the filtering method for optimizing the sizing of the electric system without discussing the fluctuation in SC voltage and other battery parameters under a high transient load current. Shen et al. [41] used the Karush–Kuhn–Tucker condition and a neural network-based EMS for splitting the load power between the battery and SC using a real-time strategy. The fixed frequency-filtering-based EMS was suggested, having a predefined drive cycle [42], but with a fixed cut-off frequency, but the optimal separation of power is not ensured in real driving situations. To ensure the safety of the EMS with a rapid charging system, the battery temperature and total costs caused by aging and losses were studied [43,44]. Besides efficiency concerns, the major problem for real-time applications is to ensure the safe operation of the system. It is essential to actively control the voltage of the SC according to the variations in the driving cycle to fulfill the requirement for all possible driving conditions. Therefore, controlling the SC voltage and adaptive frequency distribution is very important for a reliable, safe, and an efficient system.

This paper proposes a real-time EMS consisting of an adaptive charging controller for a SC and an adaptive low-pass filter (A-LPF) for a battery–supercapacitor semi-active HESS. The proposed charging controller uses an adaptive proportional integrator (API) to protect the SC from overcharging. The A-LPF uses an FLC to generate the optimal power for each source to fulfill a continuous load power-demand and keep the DC bus voltage constant. The mathematical models of the proposed EMS for the semi-active HESS were developed and simulated using MATLAB Simulink (2019a, MathWorks, Natick, MA, USA). Three drive cycles were utilized to validate the proposed technique. The simulation results of the proposed EMS (A-LPF + API) were compared with an FF-P EMS, an A-LPF with a proportional integrator derivative (PID) charge controller (PID EMS), and a BEV. The comparative analysis was carried out for different parameters, such as battery power losses, SOC and the voltage of the battery, the battery root mean square (RMS) current reduction ratio, and battery temperature.

The rest of the paper is organized into four sections. Section 2 outlines the methodology of the proposed system. Section 3 presents the simulation results and Section 4 discusses the results. Section 4 concludes the paper.

2. Methodology

2.1. Modeling

2.1.1. Supercapacitor Modeling

The conventional and simplest equivalent circuit, but still very accurate modeling of a SC, has one resistance in series and one in parallel with the capacitor [35,45]. Figure 2 represents the equivalent RC circuit.

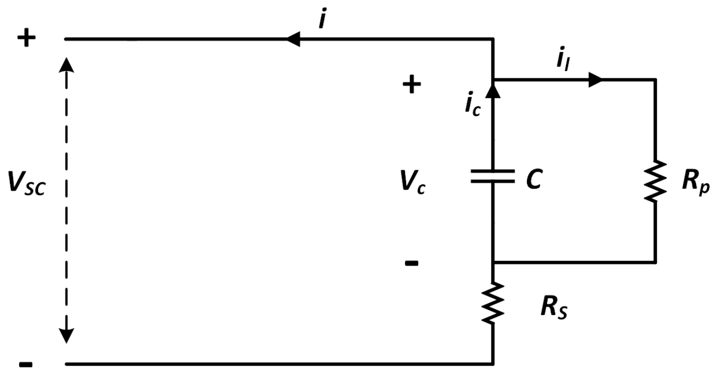

Figure 2. The equivalent electrical circuit of the supercapacitor.

The performance of the SC may be represented by the terminal voltages (V_{SC}) during discharge and charge with different current rates [46]. In the equivalent circuit, the key components are the parallel leakage resistance R_p, series resistance R_s, capacitance C, and the variables are the terminal voltage V_{sc}, terminal current i, capacitor voltage V_c, capacitor internal current i_c, and leakage current i_l. The model represents the leakage effects that impact the SC performance in long-term energy storage [47]. The equivalent series resistance and capacitance is the main component in this equivalent circuit. The mathematical modeling of the SC is given in Equations (1)–(3) [48]:

$$V_{sc} = V_c - i \times R_s, \tag{1}$$

$$dV_c/dt = \frac{-i_c}{C}, \tag{2}$$

and the leakage current (i_l) can be expressed as:

$$i_l = V_c/R_p. \tag{3}$$

The SOC of the SC (SOC_{sc}) is defined as the ratio of the voltage of the SC (V_{sc}) to its maximum voltage of SC (V_{sc_max}). The SOC_{sc} is calculated using [37]:

$$\mathrm{SOC_{sc}} = (V_{\mathrm{sc}}/V_{\mathrm{sc\_max}})^2 \times 100. \tag{4}$$

Table 1 presents the main parameters of the SC model used in this paper.

Table 1. Parameters of the supercapacitor model.

Parameter	Values (Unit)
Capacitance (C)	2700 (F)
Series Resistance (R_s)	0.7 (mΩ)
Rated Voltage (V_{sc})	2.7 (V)
Series Resistance (R_p)	1 (kΩ)

2.1.2. Battery Modeling

The battery is the main ESS for an EV, which is connected directly to a DC bus in a semi-active HESS. The charging and discharging of the battery considerably depends on various parameters, such as temperature (T) and the SOC of the battery (SOC_{bat}) [35]. The first-order resistor and capacitor (RC) network, as shown in Figure 3, was used to handle the trade-off between the modeling accuracy and complexity [49,50]. The Thevenin equivalent circuit base for a simple resistive and capacitive circuit model with a voltage source was developed using ADVISOR [51,52]. V_{ocv} is the open-circuit voltage, and R_{in} is the battery's inner resistance. For transient behavior, the resistance (R_{ap}) and capacitance (C_{ap}) were connected as a parallel network. The electrical behavior of the battery can be expressed using the following equations [53]:

$$C_{ap}\frac{dV_p}{dt} + \frac{V_p}{R_{ap}} = I_L, \tag{5}$$

$$V_t = V_{ocv} - V_p - I_L R_{in}. \tag{6}$$

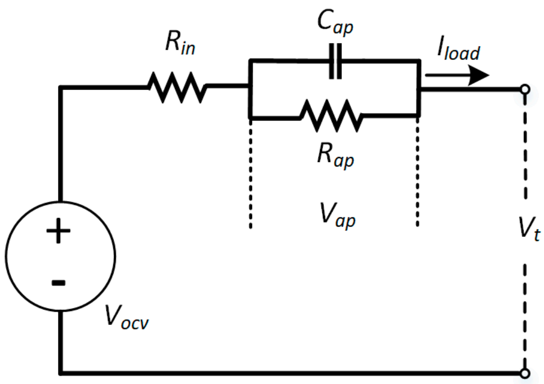

Figure 3. Schematic diagram of the battery model.

Using this model, we can compare and calculate the power losses in a BEV and semi-active HESS. The RMS current gives a rough estimation of the relative ohmic loss of the internal resistance. The reduction ratio is presented as a percentage below [54]:

$$\text{Battery current reduction ratio} = \left(\frac{\sqrt{\frac{1}{T}\int_0^T I_{bat}^2 \times dt}}{\sqrt{\frac{1}{T}\int_0^T I_{load}^2 \times dt}} \right) \times 100 \tag{7}$$

To calculate the SOC_{bat} variation, the change in charge (ΔQ), and the initial SOC ($SOC_{bat}(0)$) of the battery is required. For ΔQ, the battery current is integrated as follows [55]:

$$SOC_{bat}(t) = SOC_{bat}(0) + \int \frac{1}{C} \times I_{bat} \times dt. \tag{8}$$

Generally, the heat generation in the battery can be categorized as a resistive heat and the entropic heat. In this paper, only the resistive heat (Q_{gen}) was considered for simplicity and it can be expressed as [56]:

$$Q'_{gen} = (V_{ocv} - V_t)\, I_{load}. \tag{9}$$

After calculating the heat generation within the battery, the temperature rise can be calculated as follows [57]:

$$Q'_{gen} - Q'_c = m\, C_P \frac{\partial T}{\partial t}, \tag{10}$$

where m, C_P, Q'_{gen}, and Q'_c are the mass, specific heat capacity, rate of heat generation, and rate of convection heat, respectively. Table 2 presents the main parameters of the battery model used in this paper.

Table 2. Modeled battery parameters.

Parameter	Values (Unit)
Single Cell Voltage (V_t)	3.6 (V)
Internal Resistance (R_{in})	8.9 (mΩ)
Capacitance (C_{ap})	34.9818 (F)
Parallel Resistance (R_{ap})	24.1 (mΩ)

2.1.3. Electric Vehicle Model

Table 3 presents the main parameters of the practical EV model used in this paper [58]. The DC bus voltage (V_{DC}) was assumed to be constant, and the inverter efficiency was considered to be 90%. The force from the road grade was zero as the road gradient was zero. The load power of the EV is as follows [59]:

$$P_{load} = \left(\frac{v}{\eta}\right) \times \left[\left(m + \frac{j_{wheel}}{r_{wheel}^2}\right)\frac{dv}{dt} + F_r + F_d\right]. \tag{11}$$

The tire rolling resistance F_r is:

$$F_r = C_r \times m \times g \times \cos\theta. \tag{12}$$

The drag force F_d can be calculated using:

$$F_d = 0.5 \times \rho \times A_f \times C_d \times v^2. \tag{13}$$

As the DC bus/battery voltage was almost constant, load current is given as [60]:

$$I_L = \frac{P_{load}}{V_{DC}}. \tag{14}$$

Table 3. The key parameters of an electric vehicle.

EV Characteristic (Symbol)	Values (Unit)
Vehicle mass (m)	500 (kg)
Inertia (j_{wheel})	0.5 (kg·m^2)
Rolling resistance coefficient (C_r)	0.015
Rolling resistance coefficient (C_r)	1.25 (kg·m^{-3})
Aerodynamic drag coefficient (C_d)	0.51
Front Area (A_f)	2.4 (m^2)
Wheel radius (r_{wheel})	0.26 (m)
Road grade (θ)	0 (°)
Efficiency (η)	95 (%)
Vehicle Speed (v)	NYCC, Artemis, and NY Comp (km/h)

2.2. The Proposed Strategy of the Energy Management System

The proposed strategy used two adaptive controller-based EMSs for the battery–supercapacitor semi-active HESS. The EMS contained an API controller, which protected against deep discharging and over-charging, and the A-LPF-based controller, which was responsible for providing optimal power sharing according to the SOC_{SC} and load current, as shown in Figure 4. The I_{bas_corr} was the function that adjusted the battery current when the DC–DC converter reached its maximum current.

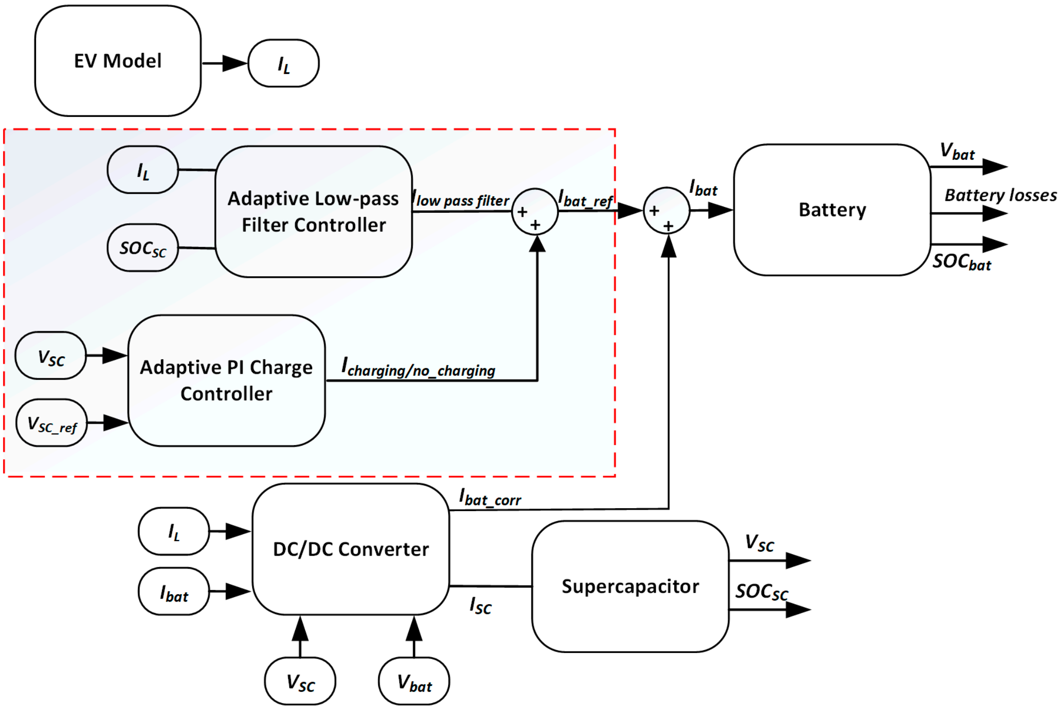

Figure 4. Overview of the proposed energy management system. EV: electric vehicle, PI: proportional integrator.

2.2.1. Fuzzy Logic Controller Architecture

Looking at the hybrid EMS as a nonlinear and time-varying system, a fuzzy logic controller was the most logical strategy for the problem. The FLC was classified into four parts, as shown in Figure 5 [61,62]. (1) Fuzzifier: In a fuzzifier, linguistic fuzzy sets are obtained from the true value of the membership function. (2) Fuzzy rule base: the fuzzy rule base is designed from professional experience and controls the system operation. (3) Fuzzy interface engine: the fuzzy linguistic input is transformed into a fuzzy linguistic output with respect to the controlled law stated in the fuzzy rule set. (4) Defuzzifier: the linguistic fuzzy set is converted to the true value using the membership function. The control signal is the control output of the FLC. It collects the system performance, matches it with the reference crisp input x(t), and decides what the system input y(t) would be to assure performance objectives.

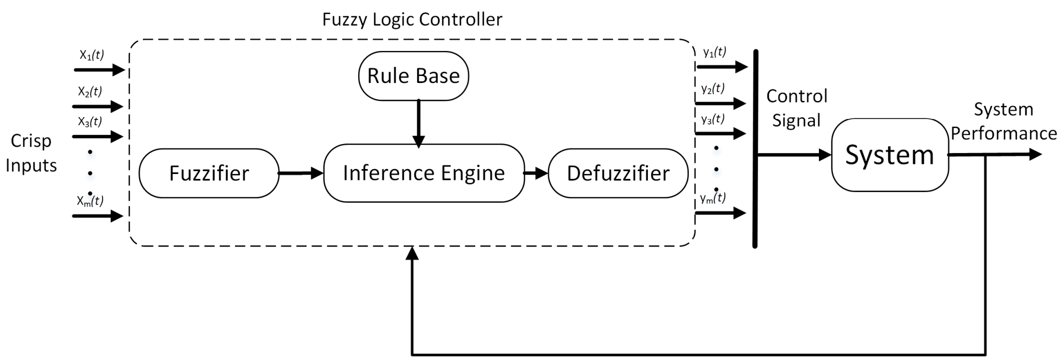

Figure 5. Overview of the fuzzy logic controller in a controlled system.

2.2.2. The Adaptive Charging Controller for SC

To operate the HESS during long drive cycles and steady-state situations, the SC should be charged using a low-power load. After every drive cycle, the charging must guarantee that the final voltage of the SC will be close to the initial SC voltage. SC's cells are very susceptible to over- and under-voltages, which require special protection in an HESS [63]. The charge of the SC is not allowed to go down below

70% to 50% of the maximum voltage [18,64]. Andersson et al. [54] use a proportional controller, but it did not update according to the drive cycle. For this purpose, we used the API controller. During low or no-load currents, the battery charged the SC to a specified value using an API controller with a fixed reference voltage (V_{SC_ref}). This controller was used to control the voltage of the SC and create margins for regenerative braking. The battery will charge the SC if the voltage of SC is very low (undercharging) and will make the SC current equal to zero until braking or deceleration. Then the overall discharge current of the battery will be the combination of the low-pass filter current and the charging current.

Figure 6 represents API, in which K_1 and K_2 are the tuning gains for the PI controller. According to the error $\mu(t)$, the desired PI controller performance is improved by updating the gains. The difference between the V_{SC_ref} and V_{SC} was adapted using an FLC for the desired charging performance. The linguistic variables are small, medium, and large, as shown in Figure 7. For the PI controller to be adaptive using fuzzy rules: If $|\mu(t)|$ is small, then K_1 is large, and K_2 is medium; if $|\mu(t)|$ is medium, then K_1 is large, and K_2 is small; and if $|\mu(t)|$ is large, then K_1 and K_2 are large.

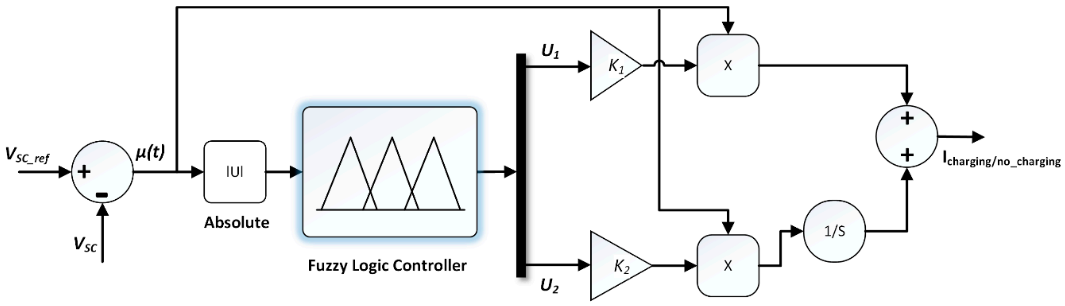

Figure 6. The adaptive charge controller for supercapacitor.

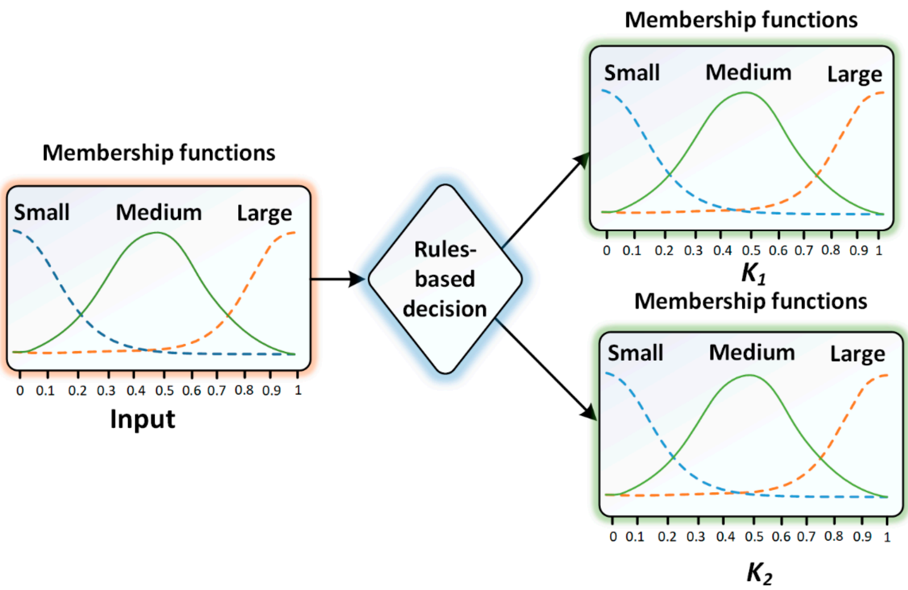

Figure 7. The membership function of the fuzzy logic controller for the adaptive charge controller.

The Gaussian membership function was utilized in the rules, which depends on two variables, namely the variance σ_i or standard deviation and center d_i as follows:

$$\mu(x) = \exp\left(-0.5\left(\frac{x_i - d_i}{\sigma_i}\right)^2\right). \tag{15}$$

The defuzzied output of the fuzzy system is fed as the gain (K_P, K_i) to the PI. Thus, the PI controller is mathematically defined as [65]:

$$v_{sc}^{*}(PI) = K_P\,\mu(t) + K_i \int \mu(t)\Gamma(t). \tag{16}$$

where $\mu(t)$ is the controller input, v_{sc}^{*} is the controller output, and K_P and K_i are the controller gains, respectively. As the gains in the PI do not change, they need to be adapted according to the system. In order to make the PI controller adaptive, the controller uses the $\mu(t)$ signal as an input for the gain parameters K_P and K_i. The FLC has one input ($|\mu(t)|$) and two output fuzzy variables U_1 and U_2, respectively. The outputs U_1 and U_2 are obtained using the center of gravity method of defuzzification. Here, U_1 and U_2 are the fuzzy controller output for the gains K_1 and K_2, respectively. Hence, the adaptation of Equation (16) using the API controller is mathematically defined as [66]:

$$v_{sc}^{*}(API) = U_1K_1\,\mu(t) + U_2K_2 \int \mu(t)\Gamma(t). \tag{17}$$

2.2.3. Adaptative Low Pass Filtering

In this controller, the demanded current is divided into a low and a high-frequency component using a low-pass filter (LPF). The transfer function of the LPF is as follows [67]:

$$H_{(S)} = \frac{1}{1 + \frac{s}{2\times\pi\times f_c}}. \tag{18}$$

The adaptive FLC is used to enhance the robustness of the variation of drive cycles. A-LPF is used to divert the high current in real-time during acceleration and deceleration from the battery to the SC using the DC–DC converter regardless of the driving condition. To make the LPF adaptive, the cut-off frequency (f_c) is continuously updated according to the load current and SOC_{SC} in the FLC circuit, as shown in Figure 8. The input variables of the FLC are the SOC_{SC} and the load current (I_L), and output is the f_c. Figure 9 presents the membership function of two inputs and the output variable of the FLC. The linguistic variables are very low (VL), low (L), medium (M), and high (H) for f_c and SOC_{sc} fuzzy variables and negative (N), positive (P), and zero (Z) are the linguistic variables for the input variable I_L [37]. In defuzzification, to transform the fuzzy outcome to a crisp output, a centroid defuzzification and min-max fuzzy inference were used [62]. During acceleration, the I_L is P, and if SOC_{SC} is H, then maximum power will be supplied by the SC, meaning f_c should be at the minimum frequency. If SOC_{SC} decreases to VL, f_c should increase. Moreover, in deceleration or braking, the I_L is N, and if SOC_{SC} is VL, then most of the regeneration power should be supplied to the SC pack for this, and f_c will be VL. If SOC_{SC} reaches H, then f_c should increase to H. When I_L is very low or zero (I_L is Z), i.e., when EV is moving at a constant low speed, then the load current will be supplied by the battery.

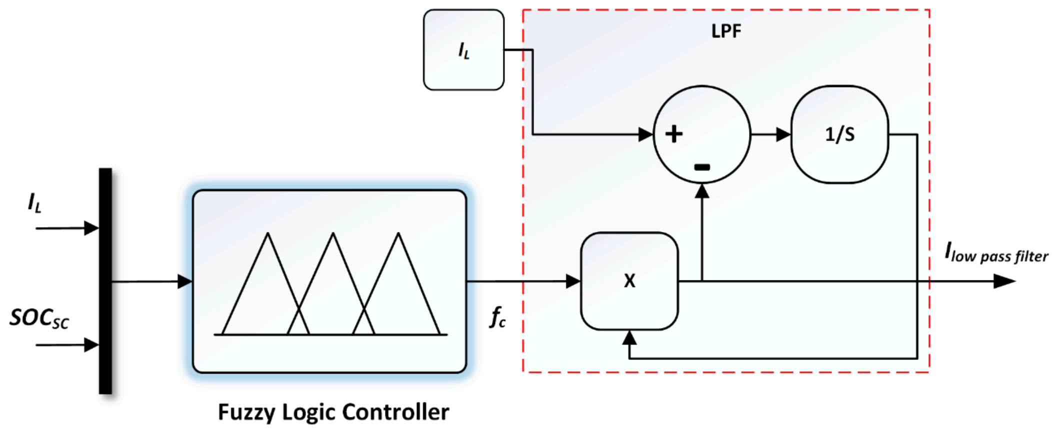

Figure 8. Simulink model of the adaptive low pass filter.

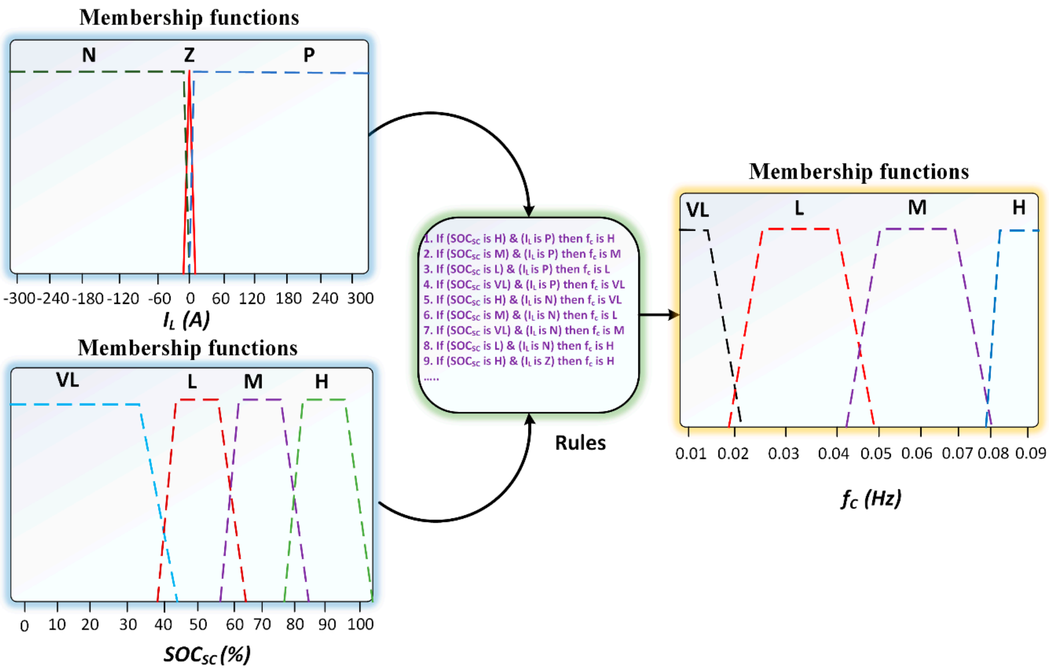

Figure 9. The membership function of the fuzzy logic control for the adaptive low-pass filter.

The A-LPF output is the optimal battery current, which is directly related to the f_c of the FLC. By using an adaptive method, this frequency can choose to minimize the battery current by intelligently deviating the load current to SC. Figure 10 shows the output surface view of the FLC for an LPF.

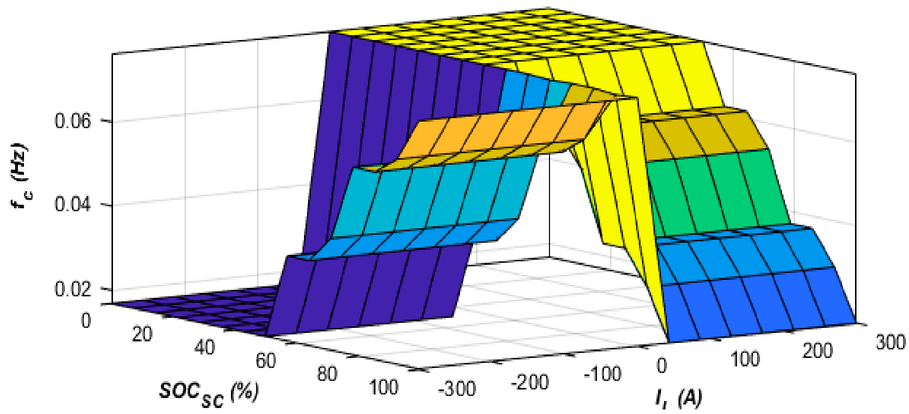

Figure 10. The fuzzy logic controller surface view of the adaptive low-pass filter.

3. Results

To evaluate the dynamic response of the proposed methodology, three standard drive cycles—the New York City cycle (NYCC), the Artemis urban (AU) cycle, and the New York composite cycle (NY Comp)—were analyzed. These cycles cover different speed ranges and have different power ranges for the same vehicle.

Figures 11–13 illustrate the simulation results of the proposed EMS using NYCC, AU, and NY Comp, respectively. Figure 11a, Figure 12a, and Figure 13a represent the speed profiles of the three drive cycles. Figure 11b, Figure 12b, and Figure 13b show the power profiles of the load, SC, and the battery in the proposed system. The power profile indicates that for high power demand, the SC provides most of the power.

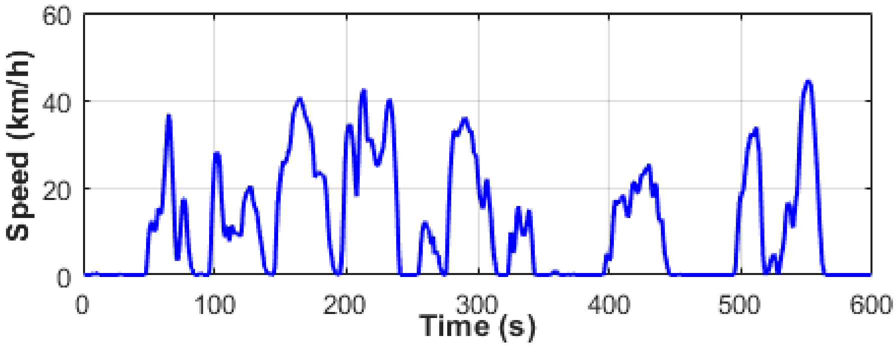

(**a**)

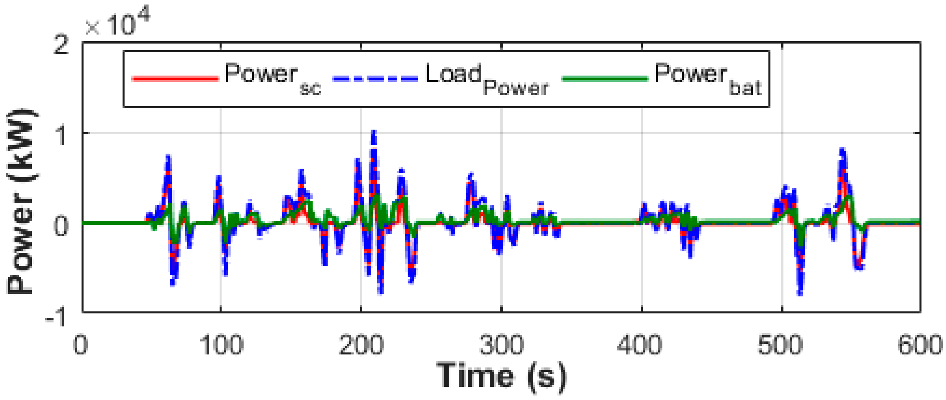

(**b**)

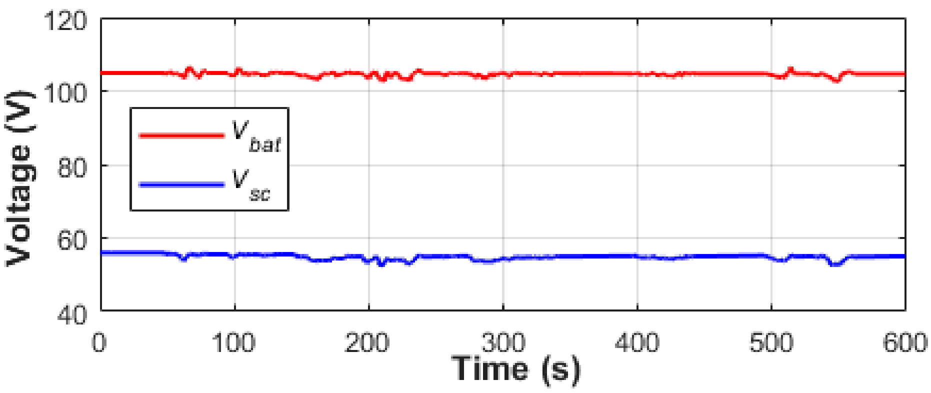

(**c**)

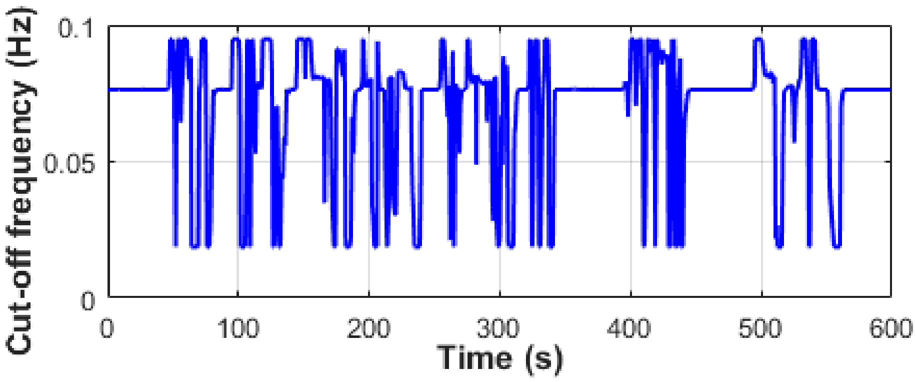

(**d**)

Figure 11. Simulation results obtained by applying the proposed energy management system (EMS) for the New York City cycle (NYCC): (**a**) speed profile; (**b**) power profile of the load, battery, and supercapacitor; (**c**) voltage of battery (V_{bat}) and supercapacitor (V_{SC}); and (**d**) adaptive cut-off frequency (f_c).

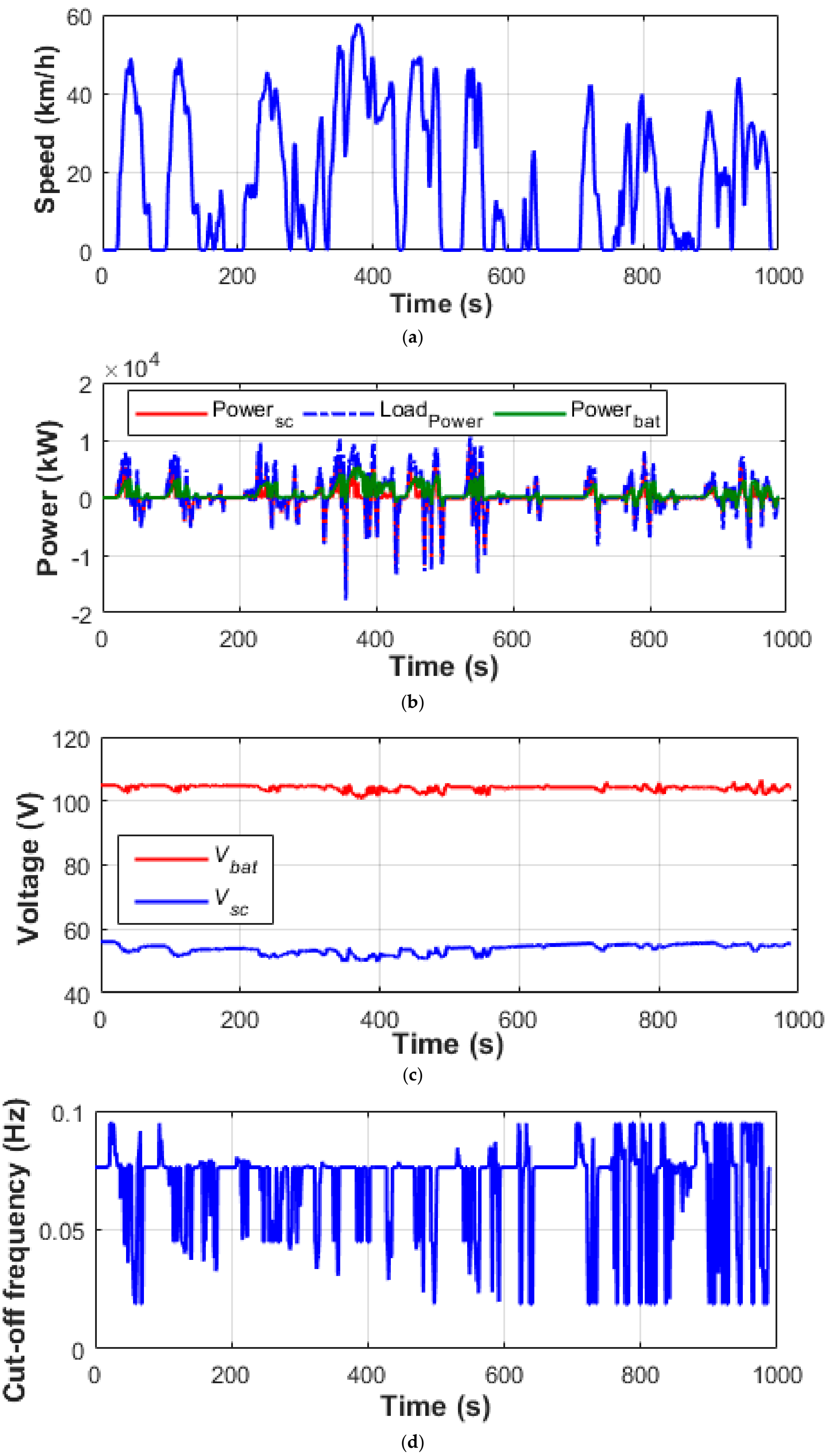

Figure 12. Simulation results obtained by applying the proposed EMS for the Artemis urban (AU) cycle: (**a**) speed profile; (**b**) power profile of the load, battery, and supercapacitor; (**c**) voltage of the battery (V_{bat}) and supercapacitor (V_{SC}); and (**d**) adaptive cut-off frequency (f_c).

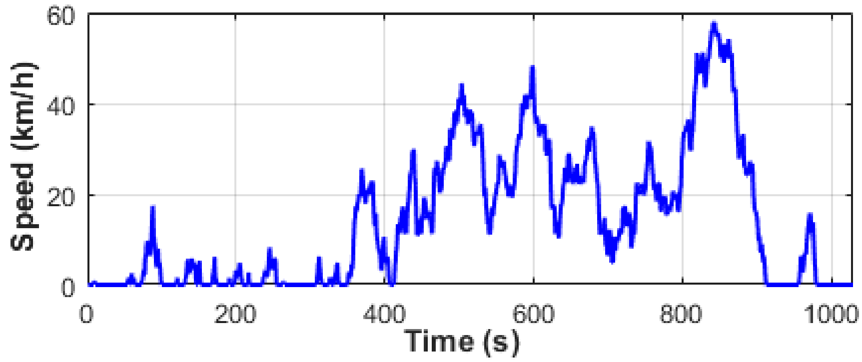

(**a**)

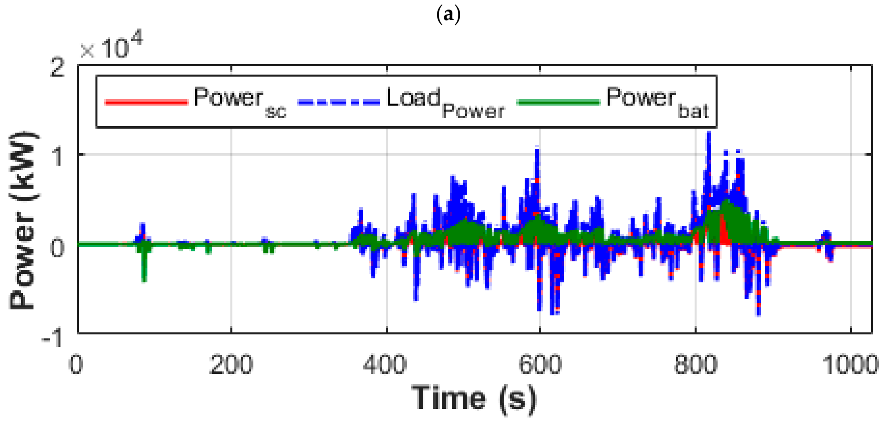

(**b**)

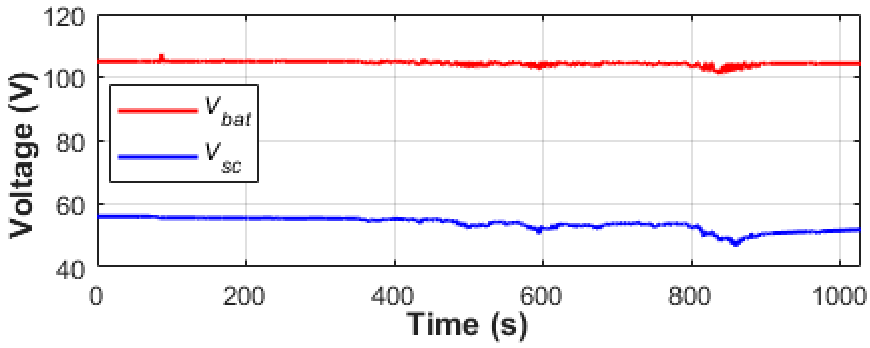

(**c**)

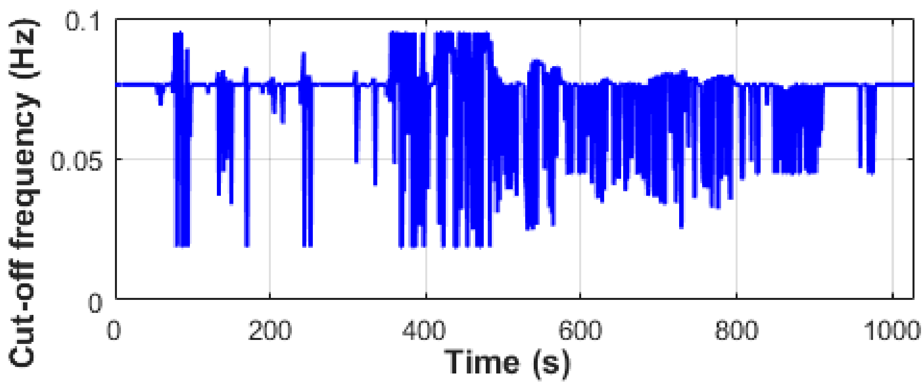

(**d**)

Figure 13. Simulation results obtained by applying the proposed EMS for the New York composite (NY Comp) drive cycle: (**a**) speed profile; (**b**) power profile of the load, battery, and supercapacitor; (**c**) voltage of battery (V_{bat}) and supercapacitor (V_{SC}); and (**d**) adaptive cut-off frequency (f_c).

Figure 11c, Figure 12c, and Figure 13c show the battery and SC voltages of the proposed EMS. The voltage of SC in the proposed system remains the same as the initial voltage at the end of every drive cycle, which indicates the stability of the proposed system. Figure 11d, Figure 12d, and Figure 13d represent an adaptation of the frequency in three drive cycles, which were according to load current and SOC_{SC} in the proposed system.

To validate the proposed strategy, the proposed EMS was compared with the online FF-P EMS, A-LPF with a PID EMS, and a BEV, using the three drive cycles. Figure 14 shows the SOC_{SC} in the proposed EMS and FF-P EMS. The SOC_{SC} in the proposed system was in the limit regardless of the harsh driving conditions of all three driving cycles, as discussed in Section 2.2.1. It did not go below 70% in all three driving conditions, which is an optimum limit [46]. Figure 14 shows that overcharging occurred in all three driving conditions (the SOC_{SC} crossed 100%) in the FF-P EMS and PID EMS because the frequency was fixed and the charging of the SC was not properly controlled for using different standard drive cycles [35,54]. It was concluded that the fixed-frequency splitting used in the FF-P EMS and not properly controlling for the SOC_{SC} in the PID EMS led to overcharging, which is very dangerous for EVs in terms of the safety of the system.

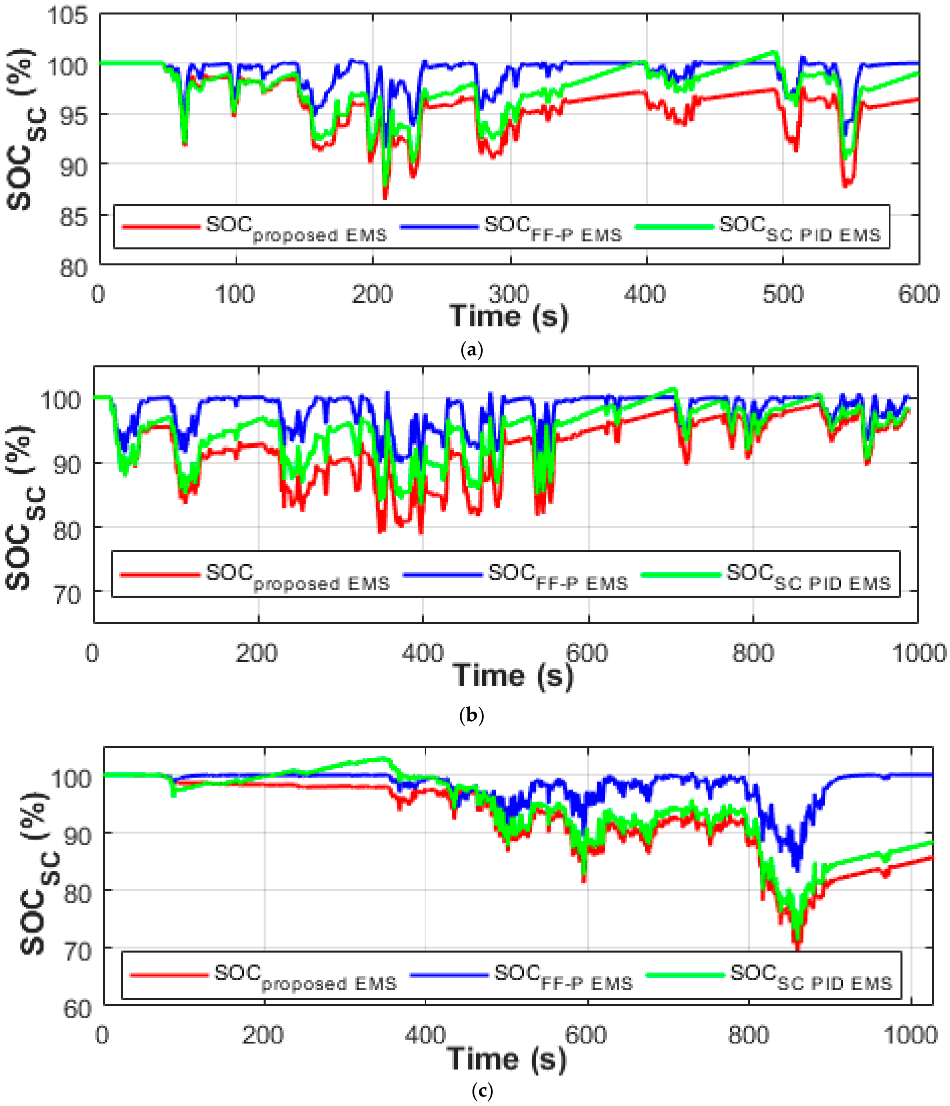

Figure 14. State of charge (SOC) of the supercapacitor (SC) in the proposed EMS, proportional integrator derivative (PID)-EMS, and fixed frequency proportional (FF-P) EMS: (**a**) SOC of SCs in the NYCC, (**b**) SOC of SCs in the AU cycle, and (**c**) SOC of SCs in the NY Comp drive cycle.

Figure 15 compares the SOC of the battery of the proposed EMS, and the FF-P EMS, PID EMS, and BEV. It shows that the battery in the proposed system had a smoother and higher battery SOC compared to other EMSs. The final SOC battery value of the proposed EMS was higher than the other three systems. The results of the SOC variations are shown in Figure A1 of Appendix A.

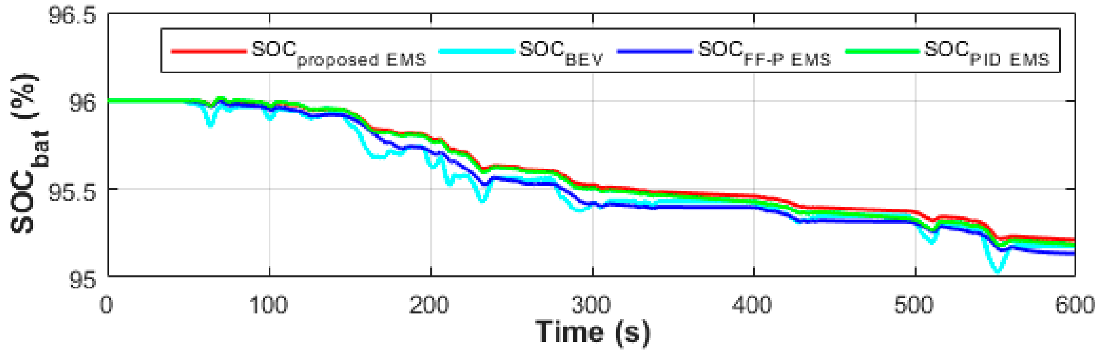

(**a**)

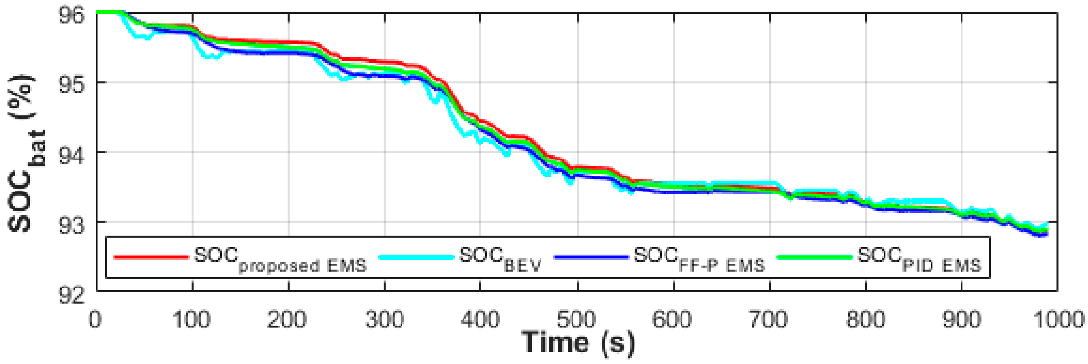

(**b**)

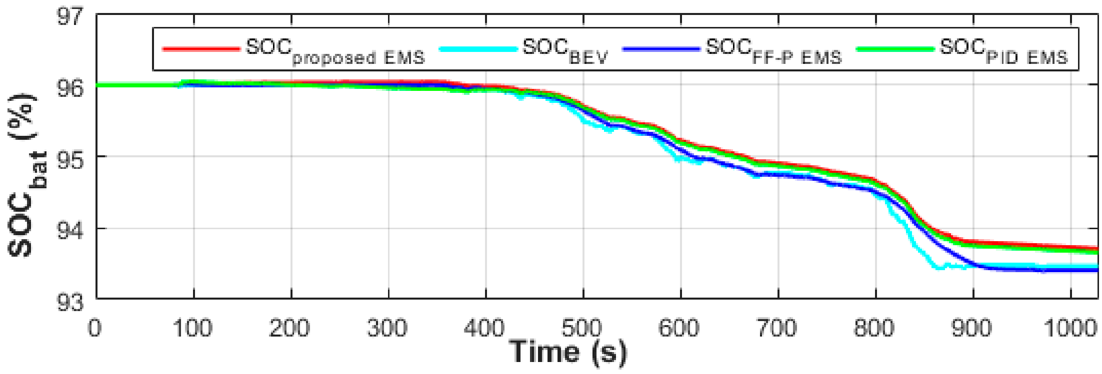

(**c**)

Figure 15. SOC of the battery in the proposed EMS, FF-P EMS, PID-EMS, and BEV: (**a**) SOC of batteries in the NYCC, (**b**) SOC of batteries in the AU cycle, and (**c**) SOC of batteries in the NY Comp drive cycle.

Figure 16 represents the battery voltages of the proposed EMS, and the FF-P EMS, PID EMS, and BEV. It shows that the battery in the proposed method was smoother and less variable compared to the other systems, which is very useful for the battery life cycle. The battery or bus voltage in the proposed strategy was almost constant compared to the other three strategies.

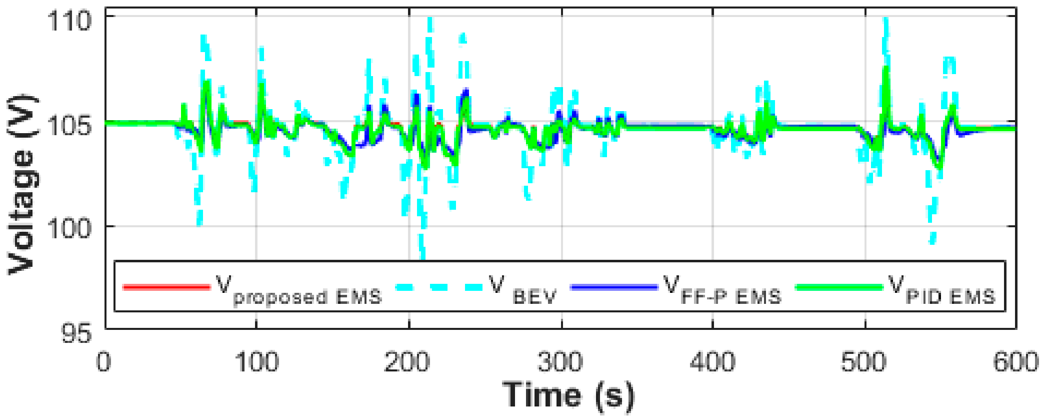

(a)

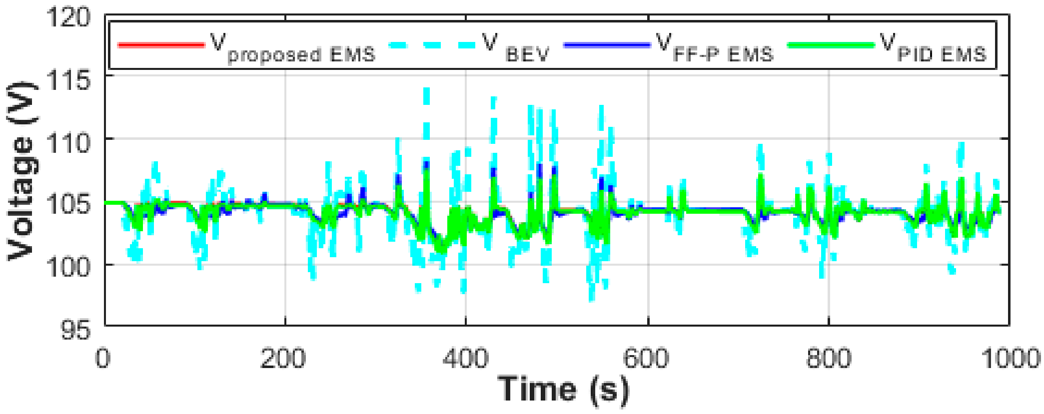

(b)

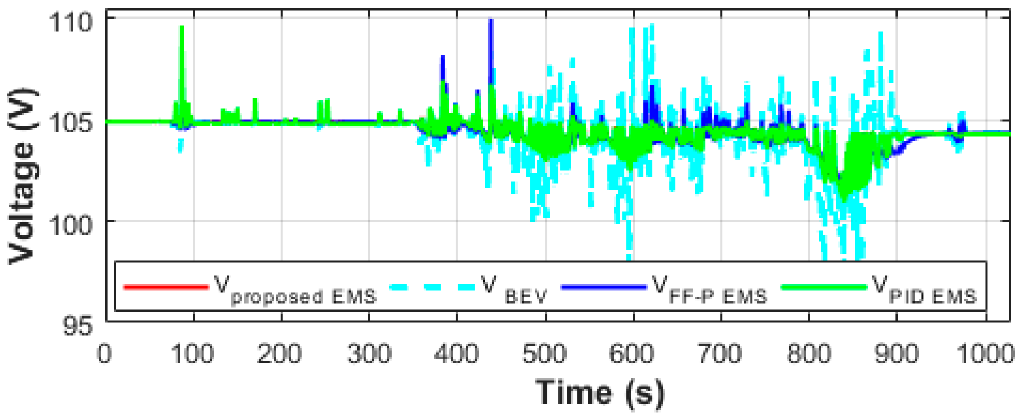

(c)

Figure 16. The battery voltages of the proposed EMS, FF-P EMS, PID-EMS, and BEV: (**a**) battery voltages in the NYCC, (**b**) battery voltages in the AU cycle, and (**c**) battery voltages in the NY Comp drive cycle.

Figure 17 presents the battery power losses in the proposed EMS, and the FF-P EMS, PID EMS, and BEV. The graphs clearly show the proposed methodology significantly reduced power losses compared to the other three methods.

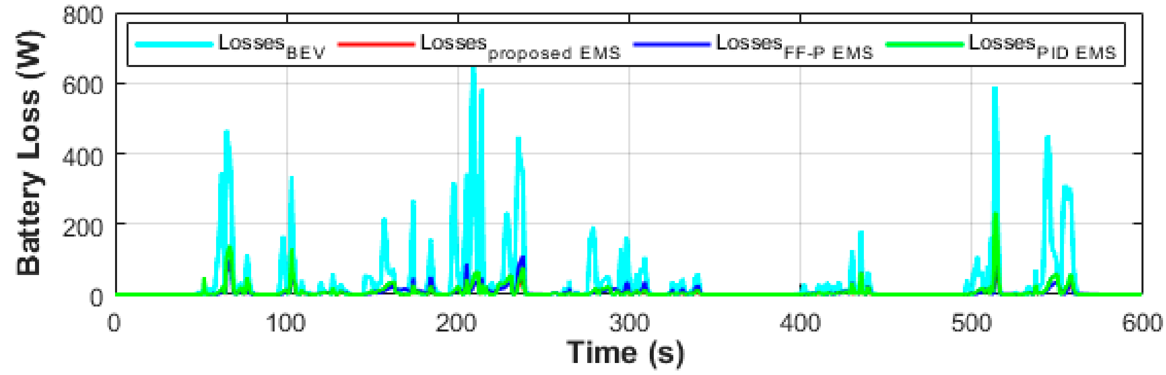

(**a**)

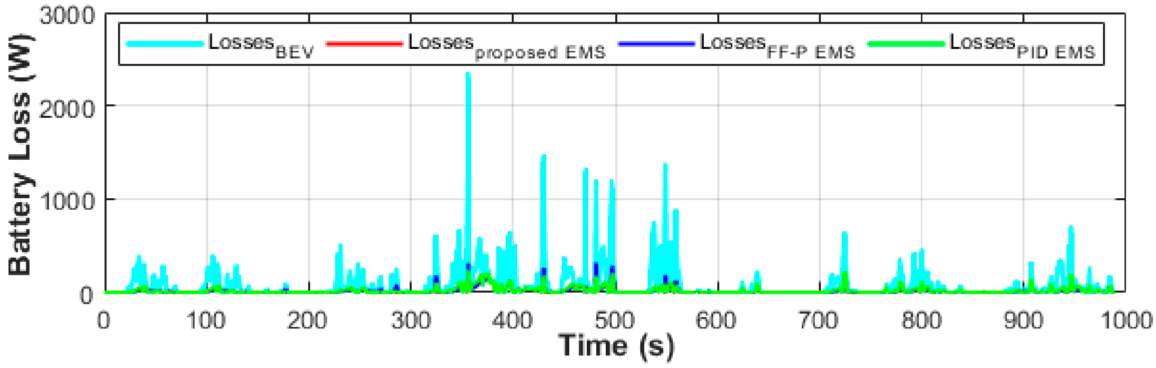

(**b**)

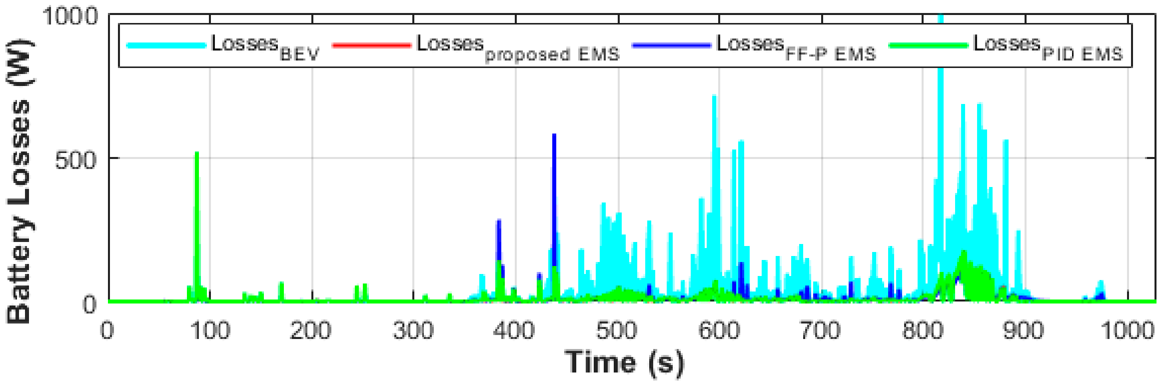

(**c**)

Figure 17. Simulation results of the battery power losses of the proposed EMS compared with the FF-P EMS, PID-EMS, and BEV: (**a**) battery losses in the NYCC, (**b**) battery losses in the AU cycle, and (**c**) battery losses in the NY Comp drive cycle.

Figure 18 shows the battery temperature of the proposed EMS, and the PID EMS, FF-P EMS, and BEV for the three drive cycles. The battery temperature of the proposed method was lower than the other systems, which is very helpful for the battery life cycle.

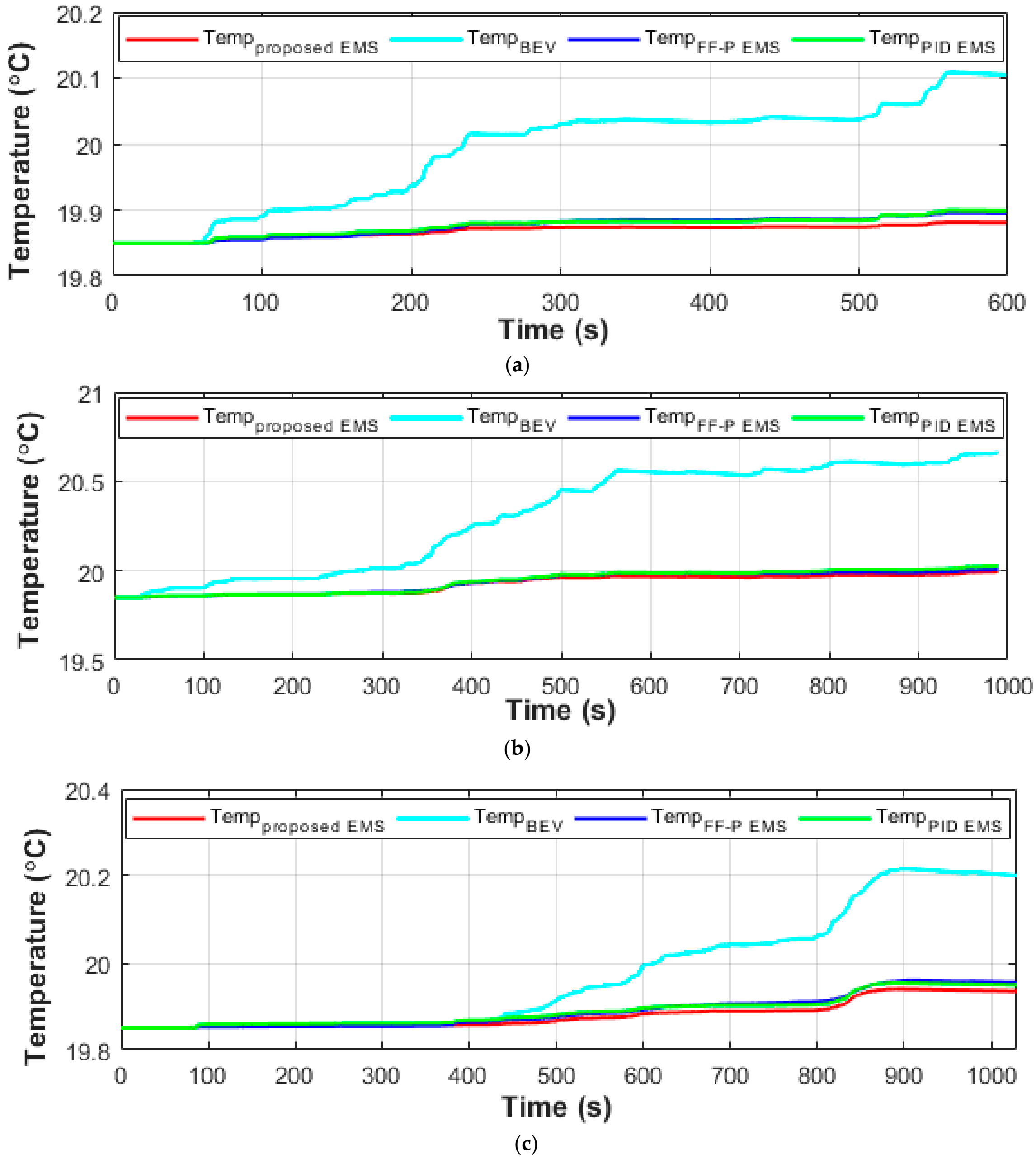

Figure 18. Simulation results of battery temperature of the proposed EMS, and the PID EMS, FF-P EMS, and BEV: (**a**) battery temperature in the NYCC; (**b**) battery temperature in the AU cycle, and (**c**) battery temperature in the NY Comp drive cycle.

The power losses in the battery of the four strategies (the proposed EMS, and the FF-P EMS, PID EMS, and BEV) were compared. The battery power losses in the BEV was the highest. The battery power loss ratio in the proposed EMS was lower than the FF-P EMS and PID EMS, as presented in Table 4. The charging performance for the proposed system is the relation between the initial voltage of SC and the average SC's voltage during each cycle. To ensure the steady state of the system, the proposed model was simulated for four repeated cycles, and the charging performance was calculated after each drive cycle, as shown in Table 2. All three drive cycles showed an almost constant charging performance value, i.e., 98%, 95%, and 96%, respectively.

Table 4. The charging performance of the proposed method and the battery power loss ratio of the proposed system, FF-P EMS, and PID EMS compared to the BEV.

Drive Cycles	Battery Power Loss Ratio of the Proposed System	Battery Power Loss Ratio of the FF-P EMS	Battery Power Loss Ratio of the PID EMS	Charge Performance of the Proposed System
NYCC	14%	18%	19%	98%, 98%, 98%, 98%
NY Comp	25%	30%	26%	96%, 95%, 95%, 95%
AU cycle	18%	19%	19%	96%, 96%, 96%, 96 %

The battery RMS current gives a rough estimation of the relative ohmic loss of the battery's internal resistance. This parameter was evaluated by comparing the battery RMS current to the load current using Equation (7). Figure 19 compares the battery current reduction ratio and total efficiency of the proposed EMS with the FF-P EMS and PID EMS for the three drive cycles.

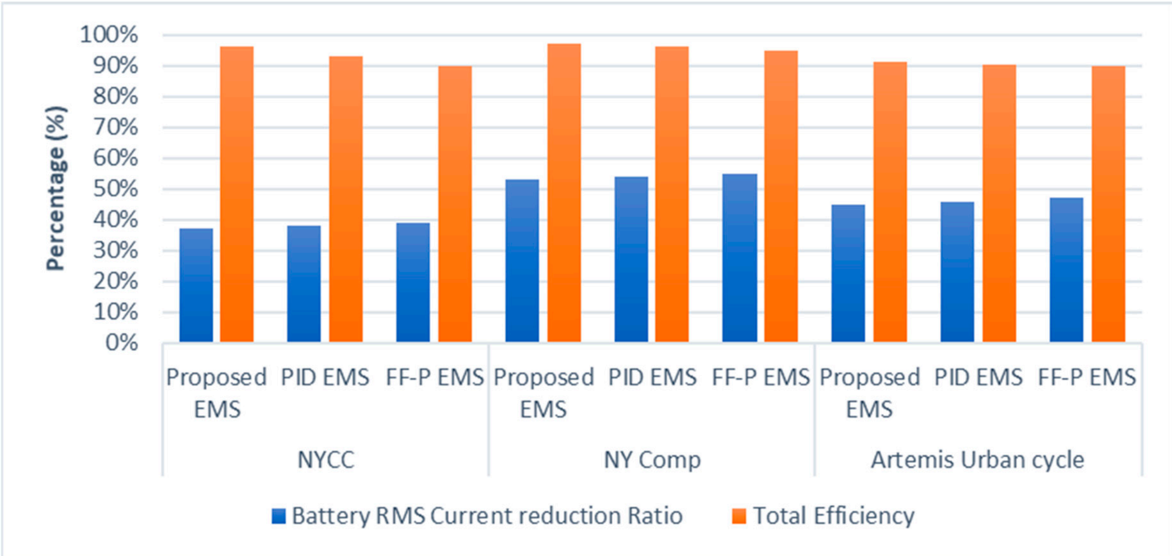

Figure 19. The battery RMS current reduction ratio and efficiency comparison of the proposed EMS, PID EMS, and FF-P EMS.

4. Discussion

The proposed EMS can prolong the battery lifetime by filtering the high-frequency power demand into the supercapacitor. Figures 11–13 confirm that the power trajectories of the battery were smoother compared to the SC and total load power. The results of the three drive cycles show that the proposed strategy prolonged the battery life significantly by reducing the peak charge/discharge power stress on the battery. The aim of adaptive frequency varying was the maximization of the effectiveness of the SC bank utilization. All the regenerative energy returned to the SC after considering the SOC_{SC}, and it enhanced the energy efficiency of the proposed system. From Figure 14, it is clear that the FF-P EMS and PID EMSs did not adapt to the change in the load power and SOC of the SC, causing overcharging during regenerative braking; however, in the proposed system, this can be successfully maintained within suitable limits and does not overcharge, which improves the reliability of the system. The SOC consumption of battery was significantly lowered compared to the FF-P EMS, PID EMS, and BEV given in Figure 15, which aids in extending the driving range of a HEV. Figure 16 shows the battery/DC bus voltage was almost constant, which is very important for transferring power to the load. As the performance and lifetime of batteries are strongly dependent on losses and temperature, Figures 17 and 18 confirmed the power losses and temperature in the proposed system was lower than the other three methods. Similarly, the battery RMS current is a reasonable demonstration of the aging parameters.

The current reduction ratio in the proposed system was less than the FF-P EMS and PID EMS for all three driving cycles. Similarly, the total efficiency of the proposed system was higher than the FF-P EMS and PID EMS, as shown in Figure 19. To ensure the steady state, the proposed model was simulated for four repeated cycles and the charge performance of the HESS was calculated to be 98%, 95%, and 96% for the three drive cycles, as shown in Table 2. These results display the stability of the proposed strategy.

5. Conclusions

An energy management system for a semi-active hybrid electric vehicle using an adaptive low-pass filter and an adaptive charging controller was implemented in this study. The charge controller was comprised of an adaptive PI controller, which ensured the safe utilization of the SC and protected it from overcharging. For optimal power-sharing between the battery and supercapacitor, an FLC-based low-pass filter was used. The stress on the battery was reduced by deviating the peak power of the load to the SC. For a short period of time, the high regenerative braking current was effectively fed to the SC for its charging. To verify the proposed EMS, three standard drive cycles (NYCC, AU cycle, and NY Comp) were used and analyzed in terms of a comparison between the proposed system and the FF-P EMS, PID EMS, and BEV. The simulation results confirmed that the proposed technique provided less variation in voltage, a small increase in battery temperature, a higher battery SOC, lower battery power losses, a higher efficiency, a reduction in the battery RMS current, and a controlled SOC of the SC as compared to the others. Also, the charging controller value of the SC displayed the steady-state charge performance of the SC for all three drive cycles.

In the future, the proposed methodology can be implemented on hardware using an FPGA or DSP TMS3200F28xx Kit and a dynamometer. The dSPACE and LabVIEW can be used for the digital signal controller board and data acquisition system. The controller code will be generated and will compile directly from the MATLAB Simulink and will then be downloaded to the dSPACE.

Author Contributions: Conceptualization, S.H., M.U.A. and H.-J.K.; Data curation, S.H.; Formal analysis, S.H., G.-S.P. and M.A.K.; Funding acquisition, H.-J.K.; Investigation, G.-S.P., S.H.N. and M.A.K.; Methodology, M.U.A. and S.H.N.; Project administration, H.-J.K.; Software, S.H. and G.-S.P.; Validation, M.U.A. and M.A.K.; Writing—original draft, S.H. and S.H.N.; Writing—review & editing, M.U.A. and H.-J.K.

Funding: This research was supported by Basic Research Laboratory through the National Research Foundations of Korea funded by the Ministry of Science, ICT and Future Planning (NRF-2015R1A4A1041584).

Acknowledgments: This research was supported by Basic Research Laboratory through the National Research Foundations of Korea funded by the Ministry of Science, ICT and Future Planning (NRF-2015R1A4A1041584).

Conflicts of Interest: The authors declare no conflict of interest.

Appendix A

Figure A1 shows the results of proposed methodology under different SOCs.

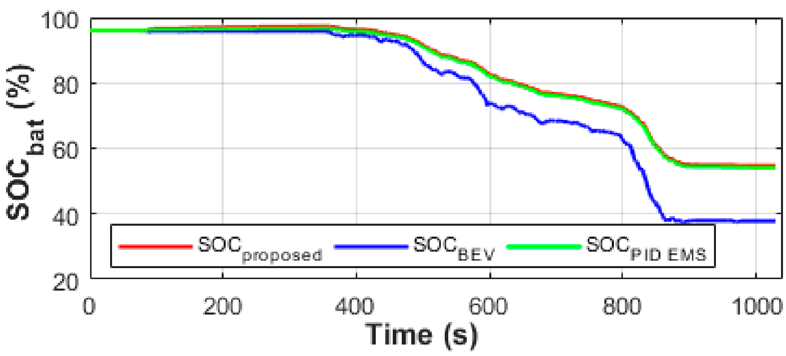

(**a**)

Figure A1. *Cont.*

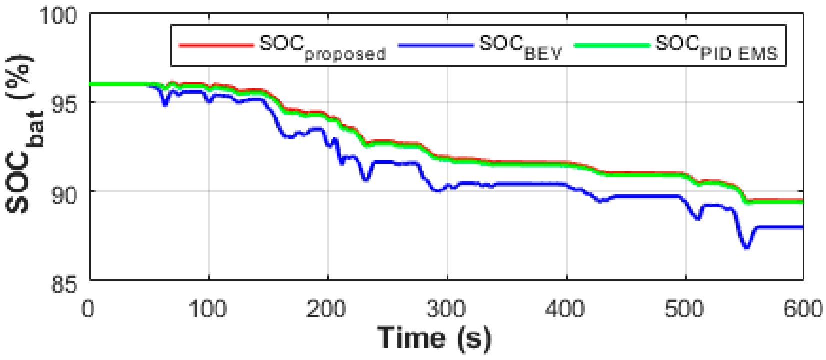

(**b**)

Figure A1. The comparison of the SOC of the battery under various drive cycles for the proposed EMS, PID-EMS, and BEV: (**a**) SOC of batteries in the NYCC and (**b**) SOC of batteries in the NY Comp drive cycle.

References

1. Erdinc, O.; Vural, B.; Uzunoglu, M. A wavelet-fuzzy logic based energy management strategy for a fuel cell/battery/ultra-capacitor hybrid vehicular power system. *J. Power Sources* **2009**, *194*, 369–380. [CrossRef]
2. Nengroo, S.; Kamran, M.; Ali, M.; Kim, D.-H.; Kim, M.-S.; Hussain, A.; Kim, H. Dual battery storage system: An optimized strategy for the utilization of renewable photovoltaic energy in the United Kingdom. *Electronics* **2018**, *7*, 177. [CrossRef]
3. Jorgensen, K. Technologies for electric, hybrid and hydrogen vehicles: Electricity from renewable energy sources in transport. *Util. Policy* **2008**, *16*, 72–79. [CrossRef]
4. Chan, C.; Wong, Y.; Bouscayrol, A.; Chen, K. Powering sustainable mobility: Roadmaps of electric, hybrid, and fuel cell vehicles [point of view]. *Proc. IEEE* **2009**, *97*, 603–607. [CrossRef]
5. Omar, N.; Monem, M.A.; Firouz, Y.; Salminen, J.; Smekens, J.; Hegazy, O.; Gaulous, H.; Mulder, G.; Van den Bossche, P.; Coosemans, T. Lithium iron phosphate based battery–assessment of the aging parameters and development of cycle life model. *Appl. Energy* **2014**, *113*, 1575–1585. [CrossRef]
6. Ali, M.U.; Zafar, A.; Nengroo, S.H.; Hussain, S.; Alvi, M.J.; Kim, H.-J. Towards a Smarter Battery Management System for Electric Vehicle Applications: A Critical Review of Lithium-Ion Battery State of Charge Estimation. *Energies* **2019**, *12*, 446. [CrossRef]
7. Karden, E.; Ploumen, S.; Fricke, B.; Miller, T.; Snyder, K. Energy storage devices for future hybrid electric vehicles. *J. Power Sources* **2007**, *168*, 2–11. [CrossRef]
8. Hussain Nengroo, S.; Umair Ali, M.; Zafar, A.; Hussain, S.; Murtaza, T.; Junaid Alvi, M.; Raghavendra, K.V.G.; Jee Kim, H. An Optimized Methodology for a Hybrid Photo-Voltaic and Energy Storage System Connected to a Low-Voltage Grid. *Electronics* **2019**, *8*, 176. [CrossRef]
9. Ali, M.U.; Zafar, A.; Nengroo, S.H.; Hussain, S.; Park, G.-S.; Kim, H.-J. Online Remaining Useful Life Prediction for Lithium-Ion Batteries Using Partial Discharge Data Features. *Energies* **2019**, *12*, 4366. [CrossRef]
10. Song, Z.; Li, J.; Han, X.; Xu, L.; Lu, L.; Ouyang, M.; Hofmann, H. Multi-objective optimization of a semi-active battery/supercapacitor energy storage system for electric vehicles. *Appl. Energy* **2014**, *135*, 212–224. [CrossRef]
11. Hussain, S.; Ali, M.U.; Nengroo, S.H.; Khan, I.; Ishfaq, M.; Kim, H.-J. Semiactive Hybrid Energy Management System: A Solution for Electric Wheelchairs. *Electronics* **2019**, *8*, 345. [CrossRef]
12. Aravindan, V.; Gnanaraj, J.; Lee, Y.-S.; Madhavi, S. Insertion-type electrodes for nonaqueous Li-ion capacitors. *Chem. Rev.* **2014**, *114*, 11619–11635. [CrossRef] [PubMed]
13. Saw, L.H.; Poon, H.M.; Chong, W.T.; Wang, C.-T.; Yew, M.C.; Yew, M.K.; Ng, T.C. Numerical modeling of hybrid supercapacitor battery energy storage system for electric vehicles. *Energy Procedia* **2019**, *158*, 2750–2755. [CrossRef]
14. Xiong, R.; Chen, H.; Wang, C.; Sun, F. Towards a smarter hybrid energy storage system based on battery and ultracapacitor-A critical review on topology and energy management. *J. Clean. Prod.* **2018**, *202*, 1228–1240. [CrossRef]

15. Liu, H.; Wang, Z.; Cheng, J.; Maly, D. Improvement on the cold cranking capacity of commercial vehicle by using supercapacitor and lead-acid battery hybrid. *IEEE Trans. Veh. Technol.* **2009**, *58*, 1097–1105.
16. Trovão, J.P.; Pereirinha, P.G.; Jorge, H.M.; Antunes, C.H. A multi-level energy management system for multi-source electric vehicles–An integrated rule-based meta-heuristic approach. *Appl. Energy* **2013**, *105*, 304–318. [CrossRef]
17. Khan, M.A.; Zeb, K.; Sathishkumar, P.; Ali, M.U.; Uddin, W.; Hussain, S.; Ishfaq, M.; Khan, I.; Cho, H.-G.; Kim, H.-J. A Novel Supercapacitor/Lithium-Ion Hybrid Energy System with a Fuzzy Logic-Controlled Fast Charging and Intelligent Energy Management System. *Electronics* **2018**, *7*, 63. [CrossRef]
18. Song, Z.; Hofmann, H.; Li, J.; Hou, J.; Han, X.; Ouyang, M. Energy management strategies comparison for electric vehicles with hybrid energy storage system. *Appl. Energy* **2014**, *134*, 321–331. [CrossRef]
19. He, H.; Xiong, R.; Zhao, K.; Liu, Z. Energy management strategy research on a hybrid power system by hardware-in-loop experiments. *Appl. Energy* **2013**, *112*, 1311–1317. [CrossRef]
20. Hung, Y.-H.; Wu, C.-H. An integrated optimization approach for a hybrid energy system in electric vehicles. *Appl. Energy* **2012**, *98*, 479–490. [CrossRef]
21. Choi, M.-E.; Kim, S.-W.; Seo, S.-W. Energy management optimization in a battery/supercapacitor hybrid energy storage system. *IEEE Trans. Smart Grid* **2012**, *3*, 463–472. [CrossRef]
22. Herrera, V.I.; Gaztañaga, H.; Milo, A.; Saez-de-Ibarra, A.; Etxeberria-Otadui, I.; Nieva, T. Optimal Energy Management and Sizing of a Battery—Supercapacitor-Based Light Rail Vehicle With a Multiobjective Approach. *IEEE Trans. Ind. Appl.* **2016**, *52*, 3367–3377. [CrossRef]
23. Jing, W.; Lai, C.H.; Wong, S.H.W.; Wong, M.L.D. Battery-supercapacitor hybrid energy storage system in standalone DC microgrids: A review. *IET Renew. Power Gener.* **2016**, *11*, 461–469. [CrossRef]
24. Biasini, R.; Onori, S.; Rizzoni, G. A near-optimal rule-based energy management strategy for medium duty hybrid truck. *Int. J. Powertrains* **2013**, *2*, 232–261. [CrossRef]
25. Bianchi, D.; Rolando, L.; Serrao, L.; Onori, S.; Rizzoni, G.; Al-Khayat, N.; Hsieh, T.-M.; Kang, P. Layered control strategies for hybrid electric vehicles based on optimal control. *Int. J. Electr. Hybrid. Veh.* **2011**, *3*, 191–217. [CrossRef]
26. Santucci, A.; Sorniotti, A.; Lekakou, C. Power split strategies for hybrid energy storage systems for vehicular applications. *J. Power Sources* **2014**, *258*, 395–407. [CrossRef]
27. Masih-Tehrani, M.; Ha'iri-Yazdi, M.-R.; Esfahanian, V.; Safaei, A. Optimum sizing and optimum energy management of a hybrid energy storage system for lithium battery life improvement. *J. Power Sources* **2013**, *244*, 2–10. [CrossRef]
28. Ansarey, M.; Panahi, M.S.; Ziarati, H.; Mahjoob, M. Optimal energy management in a dual-storage fuel-cell hybrid vehicle using multi-dimensional dynamic programming. *J. Power Sources* **2014**, *250*, 359–371. [CrossRef]
29. Liu, K.; Li, K.; Peng, Q.; Zhang, C. A brief review on key technologies in the battery management system of electric vehicles. *Front. Mech. Eng.* **2019**, *14*, 47–64. [CrossRef]
30. Armenta, J.; Núñez, C.; Visairo, N.; Lázaro, I. An advanced energy management system for controlling the ultracapacitor discharge and improving the electric vehicle range. *J. Power Sources* **2015**, *284*, 452–458. [CrossRef]
31. Wang, H.; Huang, Y.; Khajepour, A. Cyber-physical control for energy management of off-road vehicles with hybrid energy storage systems. *IEEE/ASME Trans. Mechatron.* **2018**, *23*, 2609–2618. [CrossRef]
32. Golchoubian, P.; Azad, N.L. Real-time nonlinear model predictive control of a battery–supercapacitor hybrid energy storage system in electric vehicles. *IEEE Trans. Veh. Technol.* **2017**, *66*, 9678–9688. [CrossRef]
33. Florescu, A.; Bacha, S.; Munteanu, I.; Bratcu, A.I.; Rumeau, A. Adaptive frequency-separation-based energy management system for electric vehicles. *J. Power Sources* **2015**, *280*, 410–421. [CrossRef]
34. Xiaoliang, H.; Hiramatsu, T.; Yoichi, H. Energy Management Strategy based on frequency-varying filter for the battery supercapacitor hybrid system of Electric Vehicles. In Proceedings of the 2013 World Electric Vehicle Symposium and Exhibition (EVS27), Barcelona, Spain, 17–20 November 2013; pp. 1–6.
35. Andersson, T.; Groot, J.; Berg, H.; Lindström, J.; Thiringer, T. Alternative Energy Storage System for Hybrid Electric Vehicles. In Proceedings of the 2004 Nordic Workshop on Power and Industrial Electronics (NORpie 2004), Trondheim, Norway, 13–16 June 2004.
36. Khayyam, H.; Bab-Hadiashar, A. Adaptive intelligent energy management system of plug-in hybrid electric vehicle. *Energy* **2014**, *69*, 319–335. [CrossRef]
37. Snoussi, J.; Ben Elghali, S.; Benbouzid, M.; Mimouni, M. Auto-adaptive filtering-based energy management strategy for fuel cell hybrid electric vehicles. *Energies* **2018**, *11*, 2118. [CrossRef]

38. Tokat, S.; Eksin, I.; Güzelkaya, M. New approaches for on-line tuning of the linear sliding surface slope in sliding mode controllers. *Turk. J. Electr. Eng. Comput. Sci.* **2003**, *11*, 45–60.
39. Devillers, N.; Péra, M.-C.; Bienaimé, D.; Grojo, M.-L. Influence of the energy management on the sizing of Electrical Energy Storage Systems in an aircraft. *J. Power Sources* **2014**, *270*, 391–402. [CrossRef]
40. Hammani, A.; Sadoun, R.; Rizoug, N.; Bartholomeüs, P.; Barbedette, B.; Le Moigne, P. Influence of the management strategies on the sizing of hybrid supply composed with battery and supercapacitor. In Proceedings of the 2012 First International Conference on Renewable Energies and Vehicular Technology, Hammamet, Tunisia, 26–28 March 2012; pp. 1–7.
41. Shen, J.; Khaligh, A. Design and real-time controller implementation for a battery-ultracapacitor hybrid energy storage system. *IEEE Trans. Ind. Inform.* **2016**, *12*, 1910–1918. [CrossRef]
42. Sandoval, C.; Alvarado, V.M.; Carmona, J.-C.; Lopez, G.L.; Gomez-Aguilar, J. Energy management control strategy to improve the FC/SC dynamic behavior on hybrid electric vehicles: A frequency based distribution. *Renew. Energy* **2017**, *105*, 407–418. [CrossRef]
43. Liu, K.; Hu, X.; Yang, Z.; Xie, Y.; Feng, S. Lithium-ion battery charging management considering economic costs of electrical energy loss and battery degradation. *Energy Convers. Manag.* **2019**, *195*, 167–179. [CrossRef]
44. Liu, K.; Zou, C.; Li, K.; Wik, T. Charging pattern optimization for lithium-ion batteries with an electrothermal-aging model. *IEEE Trans. Ind. Inform.* **2018**, *14*, 5463–5474. [CrossRef]
45. Zhang, L.; Hu, X.; Wang, Z.; Sun, F.; Dorrell, D.G. A review of supercapacitor modeling, estimation, and applications: A control/management perspective. *Renew. Sustain. Energy Rev.* **2018**, *81*, 1868–1878. [CrossRef]
46. Ehsani, M.; Gao, Y.; Longo, S.; Ebrahimi, K. *Modern Electric, Hybrid Electric, and Fuel Cell Vehicles*; CRC Press: Boca Raton, FL, USA, 2018.
47. Spyker, R.L.; Nelms, R.M. Analysis of double-layer capacitors supplying constant power loads. *IEEE Trans. Aerosp. Electron. Syst.* **2000**, *36*, 1439–1443.
48. Mi, C.; Masrur, M.A. *Hybrid Electric Vehicles: Principles And Applications With Practical Perspectives*; John Wiley & Sons: Hoboken, NJ, USA, 2017.
49. Ali, M.U.; Zafar, A.; Nengroo, S.H.; Hussain, S.; Kim, H.-J. Effect of Sensors Sensitivity on Lithium-Ion Battery Modeled Parameters and State of Charge: A Comparative Study. *Electronics* **2019**, *8*, 709. [CrossRef]
50. Ali, M.; Kamran, M.; Kumar, P.; Nengroo, S.; Khan, M.; Hussain, A.; Kim, H.-J. An Online Data-Driven Model Identification and Adaptive State of Charge Estimation Approach for Lithium-ion-Batteries Using the Lagrange Multiplier Method. *Energies* **2018**, *11*, 2940. [CrossRef]
51. Johnson, V. Battery performance models in ADVISOR. *J. Power Sources* **2002**, *110*, 321–329. [CrossRef]
52. Markel, T.; Brooker, A.; Hendricks, T.; Johnson, V.; Kelly, K.; Kramer, B.; O'Keefe, M.; Sprik, S.; Wipke, K. ADVISOR: A systems analysis tool for advanced vehicle modeling. *J. Power Sources* **2002**, *110*, 255–266. [CrossRef]
53. Wei, Z.; Meng, S.; Xiong, B.; Ji, D.; Tseng, K.J. Enhanced online model identification and state of charge estimation for lithium-ion battery with a FBCRLS based observer. *Appl. Energy* **2016**, *181*, 332–341. [CrossRef]
54. Andersson, T.; Groot, J. Alternative Energy Storage System for Hybrid Electric Vehicles. Master's Thesis, Department of Electric Power Engineering Chalmers University of Technology, Göteborg, Sweden, 17 October 2003.
55. Hauser, A.; Kuhn, R. Cell balancing, battery state estimation, and safety aspects of battery management systems for electric vehicles. In *Advances in Battery Technologies for Electric Vehicles*; Elsevier: Amsterdam, The Netherlands, 2015; pp. 283–326.
56. Jaguemont, J.; Boulon, L.; Dubé, Y.; Martel, F. Thermal management of a hybrid electric vehicle in cold weather. *IEEE Trans. Energy Convers.* **2016**, *31*, 1110–1120. [CrossRef]
57. Yang, Z.; Patil, D.; Fahimi, B. Electrothermal modeling of lithium-ion batteries for electric vehicles. *IEEE Trans. Veh. Technol.* **2018**, *68*, 170–179. [CrossRef]
58. Trovao, J.P.F.; Santos, V.D.; Antunes, C.H.; Pereirinha, P.G.; Jorge, H.M. A real-time energy management architecture for multisource electric vehicles. *IEEE Trans. Ind. Electron.* **2015**, *62*, 3223–3233. [CrossRef]
59. Giakoumis, E.G. Driving cycles test procedure. In *Driving and Engine Cycles*; Springer: Berlin/Heidelberg, Germany, 2017; pp. 315–345.
60. Azizi, I.; Radjeai, H. A new strategy for battery and supercapacitor energy management for an urban electric vehicle. *Electr. Eng.* **2018**, *100*, 667–676. [CrossRef]
61. Saha, S.; Ray, M.K.; Roy, P. *A Comparison between the Performance of Fuzzy Logic-Based PD Controller and General PD Controller*; OMICS International Publication: Hyderabad, India, 2012.

62. Umair Ali, M.; Hussain Nengroo, S.; Adil Khan, M.; Zeb, K.; Ahmad Kamran, M.; Kim, H.-J. A real-time simulink interfaced fast-charging methodology of lithium-ion batteries under temperature feedback with fuzzy logic control. *Energies* **2018**, *11*, 1122. [CrossRef]
63. Hadartz, M.; Julander, M. *Battery-Supercapacitor Energy Storage*; Chalmers University of Technology: Gothenburg, Sweden, 2008.
64. Cao, J.; Emadi, A. A new battery/ultracapacitor hybrid energy storage system for electric, hybrid, and plug-in hybrid electric vehicles. *IEEE Trans. Power Electron.* **2011**, *27*, 122–132.
65. Hannan, M.A.; Ali, J.A.; Mohamed, A.; Amirulddin, U.A.U.; Tan, N.M.L.; Uddin, M.N. Quantum-behaved lightning search algorithm to improve indirect field-oriented Fuzzy-PI control for IM drive. *IEEE Trans. Ind. Appl.* **2018**, *54*, 3793–3805. [CrossRef]
66. Zeb, K.; Islam, S.U.; Din, W.U.; Khan, I.; Ishfaq, M.; Busarello, T.D.C.; Ahmad, I.; Kim, H.J. Design of Fuzzy-PI and Fuzzy-Sliding Mode Controllers for Single-Phase Two-Stages Grid-Connected Transformerless Photovoltaic Inverter. *Electronics* **2019**, *8*, 520. [CrossRef]
67. Snoussi, J.; Elghali, S.B.; Outbib, R.; Mimouni, M. Sliding mode control for frequency-based energy management strategy of hybrid Storage System in vehicular application. In Proceedings of the 2016 International Symposium on Power Electronics, Electrical Drives, Automation and Motion (SPEEDAM), Amalfi, Italy, 20–22 June 2016; pp. 1109–1114.